Defense Technical Information Center Compilation Part Notice

ADP011104

TITLE: Characterization of Pulsed Vortex Generator Jets for Active Flow Control

DISTRIBUTION: Approved for public release, distribution unlimited

This paper is part of the following report:

TITLE: Active Control Technology for Enhanced Performance Operational Capabilities of Military Aircraft, Land Vehicles and Sea Vehicles [Technologies des systemes a commandes actives pour l'amelioration des performances operationnelles des aeronefs militaires, des vehicules terrestres et des vehicules maritimes]

To order the complete compilation report, use: ADA395700

The following component part numbers comprise the compilation report:
ADP011101 thru ADP011178

Characterization of Pulsed Vortex Generator Jets for Active Flow Control

Carl P. Tilmann & Kevin J. Langan
Carl.Tilmann@afrl.af.mil —Kevin.Langan@afrl.af.mil
Air Force Research Laboratory, Air Vehicles Directorate, Aeronautical Sciences Division
2130 8th Street, Wright-Patterson AFB, Ohio 45433-7542, USA

John G. Betterton & Mark J. Wilson
JGBetterton@dera.gov.uk
Defense Evaluation and Research Agency, Aerodynamics and Hydrodynamics Centre
DERA Bedford, Clapham, Bedfordshire MK41 6AE, United Kingdom

SUMMARY

The flowfields produced by several active and passive flow control devices are being investigated experimentally and numerically as part of co-operative effort between the US Air Force Research Laboratory and the UK's Defense Evaluation & Research Agency (DERA). This manuscript reports the results of an experimental investigation of pulsed vortex generator jets (PVGJs) conducted at DERA's Boundary Layer Facility in Bedford. The focus of these tests was to investigate the influence of jet velocity, pulsing frequency, and duty cycle on the mean characteristics of the flowfield produced by a PVGJ in a turbulent boundary layer. The experiments were conducted in a zero-pressure-gradient flow at a freestream velocity of 32 m/s. The flowfield was explored using a three-component laser Doppler anemometry system, and the information is used to calculate local field properties such as velocity and vorticity as well as global parameters like total circulation. The data give insight into the effectiveness of the VGs in terms of location, strength, and persistence of the generated vortices and their influence on the boundary layer. While the planned computational simulation effort is in its infancy, preliminary steady-jet computational results are compared with the flow field data that has been acquired in the boundary layer facility.

LIST OF SYMBOLS

C_μ = blowing momentum coefficient, $\Delta\ VR^2\ (\pi d_{jet}^2/4S)$
d_{jet} = diameter of the jet (normal to jet velocity vector) = 1cm
ℓ = reference length
P = static pressure
q – dynamic pressure, $\frac{1}{2}\ \rho U^2$
Re = freestream unit Reynolds number, $\rho_\infty U_\infty \ell\ /\ \mu_\infty$
F^+ = dimensionless frequency, $f\ell\ /\ U_\infty$
S = reference area
T = temperature
U = mean velocity vector
u,v,w = mean Cartesian velocity components
VR = pulse velocity ratio, $V_{jet,max}/V_\infty$
x,y,z = Cartesian coordinates
y^+ – inner turbulent coordinate, yu_τ/ν; $u_\tau^2 - \tau_w/\rho_w$
α = airfoil incidence or wing angle-of-attack
Γ = circulation (m^2/s)
Δ = pulse duty cycle, percentage of time that valve is open
δ = boundary layer thickness (where $U=0.95U_\infty$)
δ_0 – reference boundary layer thickness, ~60mm
ν = molecular kinematic viscosity, μ/ρ
ρ = density
β_{VG} = skew angle, incidence of solid VG to freestream.

Subscripts
t = total condition
w = wall condition
∞ = free stream condition
0 = reference condition

1 INTRODUCTION

Separation control devices are used routinely on military, commercial, and general-aviation aircraft. The most common of these devices is the solid-vane vortex generator (VG), typically used on wings to improve flight characteristics during off-design operation. These surface-mounted VGs create vortices that travel over the upper surface bringing high-energy fluid from the free-stream into the boundary layer. This energizes the boundary layer making it much more resistant to flow separation. The separation point is forced further aft along the wing chord, or even eliminated. One operational benefit is that separation is delayed to higher angles of attack, increasing the maximum available lift for maneuver, or permitting flight at lower airspeeds with improved control authority.

While these devices are popular for the aerodynamic and handling improvements they provide, they are generally not an optimal solution. This is primarily due to their unalterable nature once they are installed, and their associated parasite drag. It would be advantageous to have a system that has the same benefits, but could be "deactivated" while not in use. Better yet would be a system that could be actively "tuned" to the specific operating condition to overcome whatever performance deficiency it is experiencing. One might also contemplate using separation to an advantage, if it could be reliably and predictably controlled in a closed-loop manner. These considerations have led to the development of numerous varieties of pneumatic VGs.

1.1 Pulsed Vortex Generator Jet Background

The pulsed vortex generator jet (PVGJ) concept for separation control was initially based on a previously developed method of producing streamwise vortices using transverse air jets, usually called vortex generator jets (VGJs). Since first conceived in the early 50's[1], steady-blowing techniques have been studied extensively[2,3,4,5,6] and are still being investigated today[7,8,9,10]. Most of the recent investigations have been aimed at optimizing the jet orientations and orifice shapes for specific applications. In this method, steady jets are pitched to the surface and skewed to the freestream to generate vortices somewhat similar to those produced by solid VGs. Early research showed that blowing through discrete jets located near the leading edge of an airfoil could impede separation. This is achieved by energizing the boundary layer through turbulent mixing of the high-speed external fluid into the low-speed boundary layer fluid, causing an increase in the boundary layer momentum flux. It has been shown that this interaction causes the formation of longitudinal vortices similar to those produced by solid VGs, which are largely responsible for the mixing and increased resistance to separation. Johnston[11] has recently published an excellent review paper of the progress made in this area.

Pulsing the jet was first considered as a means to reduce the mass-flow requirements of the steady jet, while possibly enhancing the mixing process. The PVGJ concept has been developed in various places for several specific applications. Its developmental history at the Air Force Research Laboratory (AFRL) has primarily been aimed at separation control over

Paper presented at the RTO AVT Symposium on "Active Control Technology for Enhanced Performance Operational Capabilities of Military Aircraft, Land Vehicles and Sea Vehicles", held in Braunschweig, Germany, 8-11 May 2000, and published in RTO MP-051.

wings and airfoils for enhanced maneuverability and off-design performance. Preliminary separation-control experiments were conducted under the Small Business Innovation Research program by McManus.[12] The primary objective of this program was to develop and test the PVGJ separation control system over a broad range of flight conditions on representative two- and three-dimensional aerodynamic surfaces. The aircraft application was control of the separation on a discontinuous leading edge flap.

Preliminary separation control experiments were conducted at low speeds on simple 'flat plate' airfoil with a 15° leading edge 'flap'[13,14]. The effects of jet diameter and spacing were examined for single and counter-rotating jet pairs located on the flap. The effects of pulsing amplitude and frequency, as well as the jet diameter spacing, were also evaluated. The time-dependent flow characteristics at the jet exit were characterized, but other diagnostics were limited to mean surface pressure measurements on the flat plate and pressure surveys of the wake.

More low speed experiments were conducted on a NACA-4412 airfoil with a flat leading edge flap to determine optimum pulsed jet operating conditions for airfoil stall suppression[15]. In these experiments, PVGJs effectively delayed stall on airfoil over large range of leading edge flap deflection angles. Compressible flow experiments were also performed at free stream Mach numbers from 0.3-0.6 on an SP215 airfoil that was modified to 'bend' at $0.25\,\overline{c}$ to form a leading edge flap. Results again indicated significant aerodynamic improvements at high angle-of-attack (α>12°) by reducing or eliminating separation. Lift was increased by up to 21% at M=0.4, and by as much as 14% at M=0.5. Lift-to-drag ratio (L/D) was increased by up to 35%.

Finally, low-speed tests were performed on a 7% scale 'lambda-wing-body configuration' fitted with embedded pneumatic jet actuators near the wing leading edge[16]. In these experiments, blowing coefficients (C_μ) of 0.007 were typical. Effectiveness was demonstrated for a range of flap settings for high-α. The system increased the maximum lift coefficient by as much as 7% and L/D by up to 17%. It was also demonstrated that asymmetric use of the pulsed jets could be used to produce substantial roll moment that increased monotonically with pulse intensity. Experiments have since been conducted[17] to study the use of PVGJs for *dynamic* stall.

All of these experiments, as well as the efforts of many others[18,19,20,21], have indicated that there is significant potential for pulsed jets and other oscillatory blowing techniques to suppress separation in a variety of environments. However, we have limited knowledge of how the time-dependent flowfield induced by the jet actually behaves, or how it interacts with the boundary layer to suppress separation more effectively than steady VGs, other than the flow visualizations of Johari & McManus[22]. In these experiments, effectiveness was quantified in terms of the degree of penetration of the jet fluid into the flow based on fluorescent dye and laser sheet visualizations.

Flow control device development and characterization are a significant part of the Aeronautical Sciences Division's technical activities in flow control.[23,24] An objective of these activities is to develop and demonstrate computational tools and analytical methods required to design active flow control systems. This will require the use of analytical models for flow control devices that are founded on a combination of theoretical, experimental, and numerical information. The experiments presented here were directed at establishing an experimental database to use in modeling and analysis efforts, and also to use as a baseline for extended computational fluid dynamics analyses. It is hoped that future CFD analysis of PVGJs will ultimately enhance our understanding of the physical mechanisms behind this form of separation control.

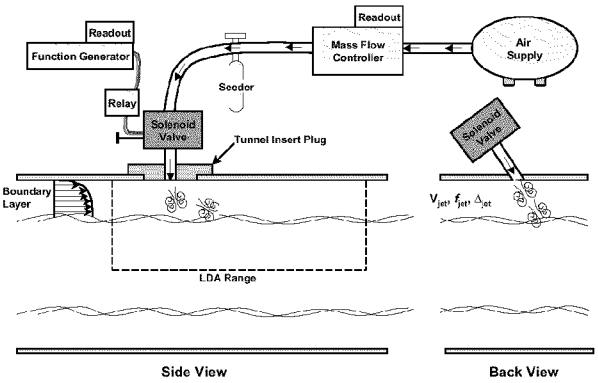

Figure 1: Schematic of experimental hardware setup.

1.2 Overview of Present Investigation

As part of a co-operative program between AFRL and the UK's Defense Evaluation & Research Agency (DERA), the flowfields around several active and passive flow control devices are being investigated. The goal of this collaboration has been to analytically and experimentally develop and validate sub-boundary layer flow control devices for future application on military aircraft wings. The AFRL share of this effort was conducted as part of a larger program aimed at improving the aerodynamic performance of military transport aircraft. This program is developing technologies necessary to develop transports to support the imminent 'Global Mobility' missions identified in the Air Force's *New World Vistas* (NWV) report.[25] The report advocates wing research which, it argues, could pay off in significantly higher aircraft efficiencies. It is our belief that emerging technologies in active flow control may provide significant improvements in aircraft performance that will extend beyond the NWV goals, enabling new classes of aircraft, and new mission capability.

Studies by DERA primarily have focused on micro-vane vortex generators and other passive sub-boundary layer flow control devices[26,27,28]. In these investigations, passive sub-boundary layer flow control devices have been tested, and limited CFD studies were conducted. In this partnership, the same experimental approaches are being used to quantify the aerodynamic effectiveness of the PVGJ active flow control concept, which has prior developmental history at AFRL.

This manuscript reports the results of the first effort in this collaboration. Specifically, recent experiments in the DERA Bedford Boundary Layer Facility directed at characterizing PVGJ flow control devices are discussed. The focus of these tests was to investigate the influence of jet velocity, pulsing frequency, and duty cycle on the mean characteristics of the flowfield produced by a PVGJ in a turbulent boundary layer. While the planned computational simulation effort is in its early stages, preliminary steady-jet solutions results are compared with the flow field data acquired in the boundary layer facility.

2 EXPERIMENTAL APPARATUS

2.1 Pulsed Jet Device

While several devices are being developed that are capable of producing pulsed jets for various applications, producing a PVGJ system suitable for controlled laboratory experiments can still be a challenge. Described below is a relatively simple apparatus that was developed and fabricated for the experiments.

The system used to generate the pulsed vortex generator jets in this experiment (Figure 1) was comprised of several off-the-shelf components. A large-volume tank supplied the pressurized air. The mean flow rate was regulated by a mass flow controller and monitored with digital readout. The pulsing was achieved with an industrial two-way solenoid valve (Figure 2). While these devices are not normally used for continuous operation, their rugged design and low response times of the smaller units

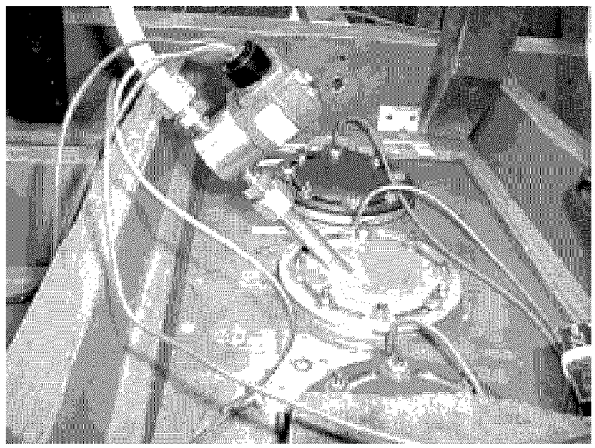

Figure 2: Photo of pulsed jet hardware used in experiment.

made them suitable for our purposes. The primary variables when selecting a valve are maximum flow rate, pressure capacity, and response time (maximum frequency). The tradeoff between size and momentum becomes significant. The larger the device is, the more sluggishly it will respond to the control signal, and sharp pulses have been found critical in previous experiments.[13] The solenoid valve chosen was a "normally closed" type that opened under AC voltage, and was pressure rated at 100psi.

The solenoid valve was controlled by a function generator that produces a square-wave voltage of appropriate magnitude and adjustable frequency and duty cycle. The usual US-UK power supply converters were also required. The valve was directly mounted to a short length of 1cm ID pipe that was run through a tunnel insert plug at 45° to the surface normal (Figure 2). The insert plug had been previously manufactured to fit into existing apertures in the ceiling of the DERA Boundary Layer Tunnel.

2.1.1 System Limitations

As mentioned above, the performance of the pulsing apparatus was primary limited by the solenoid's response time (which limited frequency and duty cycle) and the aperture size (which limited mass flow rate). The sustainable mass flow rate of the air supply was also a limitation. The maximum average mass flow that the system could maintain under any conditions was about 416slpm (0.0083 kg/sec). This yielded a maximum steady jet velocity of 88m/s. This translated to a maximum velocity ratio of 2.70 at the nominal tunnel conditions used.

It was found that if very long pulses (large duty cycles or low frequency) were attempted at high velocity ratios, the pressure in the feed line could not be maintained for the entire duration of a pulse. This caused flow to become very weak to non-existent toward the end of a pulse. Pulsing at very high frequency required the solenoid valve to respond at very short time intervals. The same limitation existed for very low duty cycles, since the response time required is proportional to Δ/f. Since the response-time of the valve was on the order of 4ms the shortest "on" cycle that we could expect the valve to achieve a relatively sharp square wave response to was about 15ms. This allowed a maximum operating frequency of 33Hz with a duty cycle of 50% (or 16Hz at 25%).

2.2 DERA Boundary Layer Facility

The experiments were conducted in DERA's Boundary Layer Facility in Bedford (Figure 3). This facility is an open-return tunnel with three 1.83m (6ft) long sections that are all 1.2m wide. The tunnel has a continuous flexible floor that permits a maximum height of 0.7m. While the adjustable floor allows the longitudinal pressure gradient to be manipulated, the present experiments have been conducted in a zero-pressure-gradient flow with a test section height of approximately 0.3m, and at a free-stream velocity of 32.6m/s. The third section is fitted with optical glass on one sidewall, and a large region of this section can be explored with a three-component laser Doppler anemometry (LDA) system to measure flowfield velocities. Flow control devices were mounted on the centerline of the tunnel roof, just downstream of the juncture between the second and third sections. In this configuration, the optical traverse could move the beams from about 10cm upstream to about 0.5m downstream of the devices.

A "jet catcher" is secured at the exit of the last section to diffuse the high velocity air to an acceptable level in the room. Physical access to the working-section is available through pairs of opening windows on either side of the tunnel. Due to the LDA seeding and tunnel noise, the manned data acquisition and control systems have been fitted outside the laboratory.

3 EXPERIMENTAL TECHNIQUES

This section will the outline the experimental techniques used to obtain raw flow data, as well as how the data was reduced to meaningful quantities representing the effectiveness of the control devices. The focus of these tests was to investigate the pulsed vortex generator jet (PVGJ) flow control device. Several pulsed and steady configurations were tested to investigate the effects of jet frequency, velocity, and duty cycle. Results from similar tests on conventional delta-vane VGs, which had been previously tested at several orientations to the flow, are used here as a baseline for comparison.

3.1 Laser Doppler Anemometer

Laser Doppler Anemometry (LDA) has been an established research technique for measuring flow velocity vectors for many years.[29] The technique uses pairs of similar intersecting laser beams defining a small measurement region in a flow. When correctly sized seeding particles are introduced into the flow stream and pass through the measurement region they reflect the probing laser beams as a short burst of light. The wavelength of this reflected light is slightly shifted proportionally to the particle velocity, due to the Doppler effect. If two similar laser beams with slightly different subtended angles to the flow illuminate the seeding particle, the Doppler shifted reflections can interfere and produce a fringe pattern within the reflected burst of light. With a known wavelength of the laser light and a known angle between the intersecting beams, a conversion factor between the Doppler frequency and the velocity can be calculated. The frequency of the fringe pattern is then measured, and the velocity component of the seeding particle perpendicular to the bisector of the two laser beams is determined. Using three correctly oriented pairs of interrogation laser beams of differing wavelength illuminating a single measurement region (and three photodetectors), it is possible to obtain three orthogonal velocity vectors at any given accessible position.

This technique has advantages over physical sensors like hot wires or pressure probes in that the only flow intrusion is that of the seeding particles used. It has been shown that for air-flow

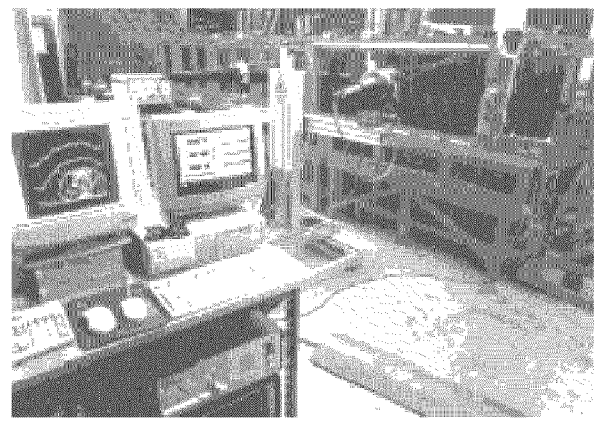

Figure 3: DERA Bedford Boundary Layer Wind Tunnel

speeds up to Mach 2 spherical oil droplet seeding particles with diameters smaller than 2μm will follow the air flow direction without significant deviation. The method's particular advantages include: non-intrusive measurement, high spatial and temporal resolution, no need for calibration, insensitivity to temperature and pressure variations, and the ability to measure in reversing flows.[30] The advantages of this optical flow measurement technique over particle image velocimetry are the very high spatial and temporal resolution.

For each configuration tested, measurements were taken with the LDA at several planes downstream of the jet. This information was used as outlined below to calculate local field properties such as velocity and vorticity as well as global parameters like total circulation. The data give insight into the effectiveness of the VGs in terms of location, strength, and persistence of the generated vortices and their influence on the boundary layer.

3.2 Data Reduction

With the mean velocity information on planes behind the jet in hand, longitudinal vorticity can be calculated in the usual way

$$\omega_x = \frac{\partial w}{\partial y} - \frac{\partial v}{\partial z} \tag{1}$$

The total circulation over the x-plane can then be calculated by integrating the vorticity over the measurement plane.

$$\Gamma_x = \iint \omega_x \, dy \, dz = -\Gamma \tag{2}$$

Here, we have defined the circulation, Γ, as positive in the rotational direction of the primary vortex to avoid any confusion when comparing to data reduced with different choice of coordinate systems, and differing experimental device orientations. Several approaches to calculating these quantities were assessed; most of which used Amtec Engineering's *Tecplot*™ data visualization package[31] to some extent.

Since the region the flow that is influenced by the jet grows in the downstream direction, the data were generally obtained at varying spanwise locations and resolutions, and over dissimilarly sized and shaped regions. This caused the collected data to be somewhat "irregular". Throughout most of the data reduction, the irregular data at each plane were interpolated onto a "regular", or "structured" mesh. This associated each data point with its neighboring points, and consequently finite-difference methods could be applied in the normal way to calculate gradients (in Equation 1). These derivatives were calculated using built-in *Tecplot* functions (2nd-order differencing). *Tecplot* integration functions were then used to calculate circulation (Equation 2). This entire process, including queries to the user regarding interpolation and plotting options, was incorporated in a single *Tecplot* macro.

Since this method was developed, Amtec Engineering's *CFD Analyzer* was available soon after, which automates the calculation of many flow variables, even on the unstructured data meshes. On a given grid, using the *CFD Analyzer* yielded the same results for vorticity and circulation that were calculated by the macro discussed above. The only differences were caused by the interpolation of the irregular data onto the regular grid. This interpolation process often helped to smoothly "fill in" spaced in the experimental data in a helpful way. However, at times it led to inconsistent estimates for field circulation, as will be discussed below.

In these experiments, the data were typically taken along vertical (y, normal to the wall) lines spaced 10mm apart in the lateral (z) direction. Each line of data had a resolution of 3.5-5.0mm, depending on the local flow gradients. In the results presented here, unless otherwise noted, the data were interpolated onto a regular mesh having resolutions of $\Delta z \times \Delta y$ =6.25×3.45mm, again depending on local flow gradients and the size of the interpolation region. At the highest jet velocity ratio (VR-4.60), the regular mesh had a resolution of 8.33×6.25mm.

4 NUMERICAL SIMULATION TECHNIQUE

The flowfield produced by steady and pulsed jets is also being numerically simulated using computational methods of varying complexity. All simulations completed to date under this effort have been for steady jets under tunnel conditions. The numerical results presented here were obtained by solving the Reynolds-averaged Navier-Stokes (RANS) equations, with the algebraic turbulence model of Baldwin and Lomax[32]. Solutions were obtained with a widely used commercial simulation package (*GASP*[33]), and the numerical results are compared to the experimental results. *GASP* is a fully conservative shock capturing code that has been widely used for the analysis of many types of flows.

4.1 Solution Strategy

The simulations were performed on relatively uncomplicated grids representing the jet issuing into a turbulent boundary layer. The entire computational mesh consisted of three computational zones, (the edges of which are shown in Figure 4) connected to each other by 2 zonal boundaries and was comprised of 575×10^3 cells. Flow information was passed through the zonal boundaries via five-point overlaps. To resolve the features of the flowfield near the jet and to provide the resolution required by the turbulence model, the grid was clustered near the jet and wall. At a location 0.2m ($20d_{jet}$) upstream of the jet, the wall grid spacing corresponded to a y^+ value of roughly 2.5, and 75% of the grid points were in the boundary layer. This dimensional wall spacing is maintained throughout the computational grid.

Adiabatic no-slip conditions and vanishing normal pressure gradient were enforced on the wall surface. The jet was modeled with a simple 'top hat' velocity profile, which has been shown to not to play a significant role in the developing vortex, provided the net momentum flux rate is maintained.[7] The jet flow was also assumed to be at ambient pressure and temperature. It was also assumed that tunnel was deep enough and wide enough to have minimal influence on the flowfield near the jet. Thus, flow variables were extrapolated from the interior at the downstream plane, and the Reimann invariants from characteristic theory are satisfied on the free-stream (top) boundary. Periodicity was imposed on the side planes to simulate a lateral row of distantly spaced co-rotating jets. Since the intent is to simulate the experiments, the data obtained from boundary layer surveys have been used for the numerical upstream boundary condition.

To allow for the specification of a two-dimensional upstream boundary condition obtained experimentally, the flow was simulated on a two-dimensional grid for a short distance (10cm) ahead of the three-dimensional simulation region. The LDA system allowed experimental data to be obtained very close to the wall, but not completely through the laminar sub-layer. The characteristics between y=0.32mm and the wall were obtained with a cubic interpolation to the no-slip wall. However, the two-dimensional region allowed the boundary layer to develop into a fully turbulent profile upstream of the three-dimensional region. Very little change in the boundary layer characteristics was

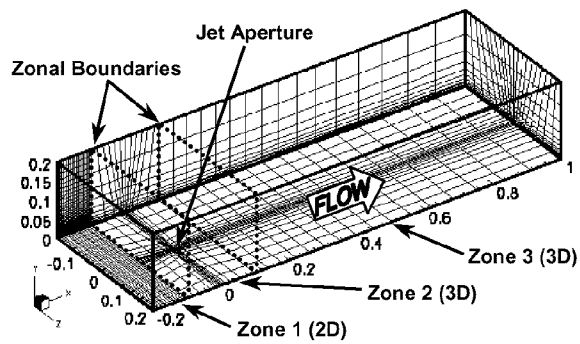

Figure 4: Grid features for numerical simulations.

observed through this region. A constant pressure was assumed through the upstream boundary layer. The two-dimensionality of the flow in the DERA Boundary Layer Facility has also been demonstrated (see Section 5.1).

Throughout the three-dimensional injection zone ($x \geq -10d$) the RANS equations were solved to 3rd-order spatial accuracy using Jacobi inner iterations[33]. The inviscid fluxes were split by the method of van Leer[34], and the min-mod limiter[35] was used. This region was comprised of two computational zones, containing a total of 574×10^3 cells.

4.2 Convergence Issues

A three-grid sequencing method was used where converged solutions were obtained on three grids of varying resolution. A converged solution is quickly obtained on the coarsest grid, then interpolated to a more refined grid. The solver is then restarted on this finer grid. In this case, groups of 8 cells (2×2×2) of the finest grid were combined to make the medium grid. This was done again to define the coarsest grid. This method not only accelerates solution convergence, but also affords an expedient means to evaluate grid consistency. Temporal convergence was demonstrated at each sequence by monitoring the progress of the solution as well as the residual vector and in time.

The computed vortical structures downstream of the jet increased in complexity and detail with each grid refinement. While the predicted flowfield was somewhat altered by the last grid refinement, the downstream flowfield and calculated forces the wall did not drastically change. Predicted integrated pressure forces over "Zone 3" normal to the surface for the two finest meshes were almost identical. However, there were 3.6% and 60% changes in the integrated lateral and longitudinal sheer stresses on the plate, respectively. This certainly indicates that grid convergence may not be achieved in the region of interest.

4.3 Computational Requirements

When using the mesh-sequencing scheme described above, the computational requirements for the calculations, both in terms of memory and computational effort, increase by approximately a factor of eight with each grid refinement. For the finest grid (574×10^3 cells), *GASP* required 7.3×10^6 Words of memory and 130 seconds/iteration on a Silicon Graphics R12000 processor.

5 RESULTS

While the floor of the tunnel is flexible to allow adjustable pressure gradients to be imposed, these experiments have been conducted with the tunnel floor tuned to maintain a flow with no longitudinal pressure gradient in the test section. While several pulsed and steady configurations were investigated to study the effects of jet pulsing frequency, velocity, and duty cycle, not every combination of parameters in Table 1 could be tested due to hardware limitations. Solid delta-vane vortex generators have previously been tested at several orientations to the flow, and are used here as a baseline for comparison.

Results obtained from the experiments and the preliminary CFD analysis are examined here with an eye toward quantifying the effectiveness of the devices based on the path, strength, and persistence of the generated vortices and their influence on the boundary layer.

5.1 Upstream Tunnel Conditions

The boundary layer was surveyed slightly upstream of the pulsed jet at several transverse locations to assess the two-dimensionality of the base flow, as well as to provide boundary conditions for numerical simulations. The measured boundary layer characteristics (Figure 5) are typical of a turbulent boundary layer under no streamwise pressure gradient.

5.2 Conventional Delta Vortex Generator Vanes

To understand the desired behavior of traditional VGs, we first will examine the flowfield influenced by a solid delta-vane VG. A few of these traditional vane vortex generators, as well as many sub-boundary layer devices of varied shape and size, had been previously investigated at DERA. These experiments were conducted in the same facility, and under almost the same conditions (U_∞=32m/s, zero pressure gradient) as the pulsed jet studies. Vanes of varying shape, size, and orientation to the flow were assessed. The results discussed are for a delta-shaped vane with a 30mm height (h) and a 70mm length at the root (67° leading edge sweep). Data were taken with the LDA at several locations behind the vane. The data are examined here using the same methods used below to characterize the PVGJs. The solid-vane data are also used here to highlight the effects of different reduction methods on the calculated quantities.

Table 1: Tunnel Conditions.

Parameter	Value
V	32.6 m/s
q	632 Pa
Re/ℓ	2.2×10^6 m^{-1}
T	294 K
f (Hz)	7.5, 15, 30
$F^+/\ell = f/U_\infty$ (m^{-1})	0.25,0.5,1.0
$VR = U_{jet}/U_\infty$	1.38, 1.84, 2.76, 4.60
Δ = Duty cycle	15, 25, 50,100%

From the field data obtained with the LDA system, we can compute the local longitudinal vorticity of the flow as discussed above. The longitudinal vorticity levels and secondary velocity vectors are shown in Figure 6 at four measurement planes downstream of the vane set at a skew angle of β_{VG}=20°. The longitudinal velocity contours are shown with secondary streamlines in Figure 7. The coordinate system origin is at the base of the fin trailing edge, with x in the longitudinal tunnel direction, and in the longitudinal tunnel direction, and y is in the direction normal to the wall. We observe that very near the vane, there are large positive and negative vorticity levels. In

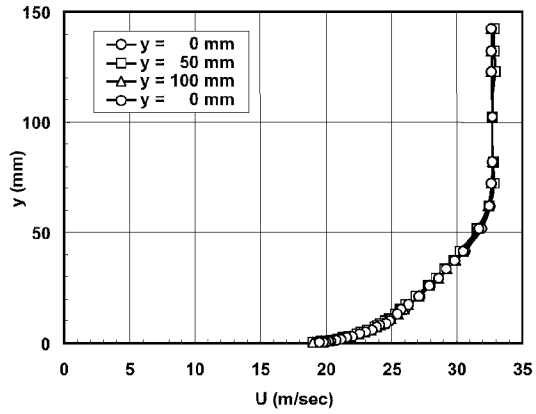

a) Mean longitudinal flow

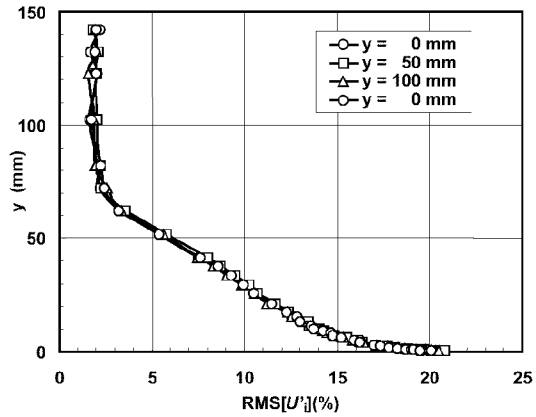

b) Turbulence intensity.

Figure 5: Measured upstream conditions (x = -10 d_j).

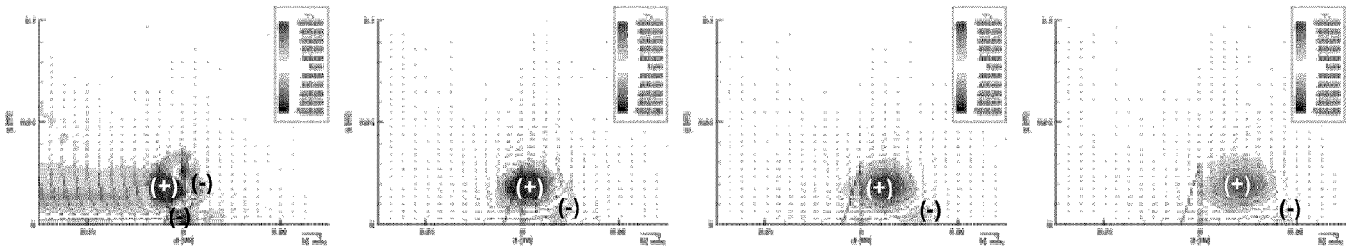

a) $x = 0.5h$ b) $x = 5h$ c) $x = 10h$ d) $x = 15h$

Figure 6: Longitudinal vorticity contours & secondary flow vectors. h=30mm; ℓ_{VG}=70mm; β_{VG}=20°.

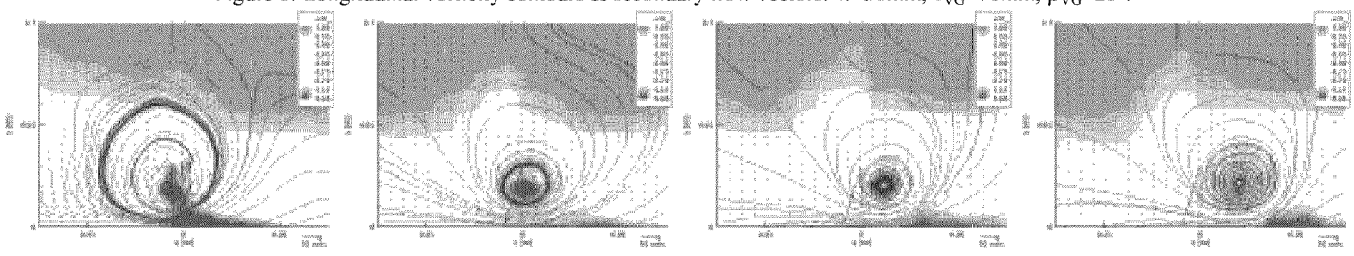

a) $x = 0.5h$ b) $x = 5h$ c) $x = 10h$ d) $x = 15h$

Figure 7: Longitudinal velocity contours, secondary streamlines. h=30mm; ℓ_{VG}=70mm; β_{VG}=20°.

this region, the effects of the vane sweeping fluid positive z-direction very near the surface can still be seen. As the vortex travels downstream, it evolves into a single coherent structure of positive circulation (+), accompanied by a much smaller and weaker region of negative circulation (–). The primary vortex is established at about $0.7h$ from the surface, and maintains this elevation as it proceeds downstream. The vortex continues to move laterally in the direction of the vane skew. Note that the peak vorticity is monotonically decreasing downstream.

The velocity contours (Figure 7) indicate that the presence of the vane significantly distorts the outer boundary layer edge. The inner boundary layer is noticeably energized on the down-flow side of the vortex, as it pulls high-energy flow in from the freestream. As discussed earlier, this is the primary mechanism for stabilizing the boundary layer, and making it more resistant to separation. A significant region of low-energy fluid is also observed in the upwash region.

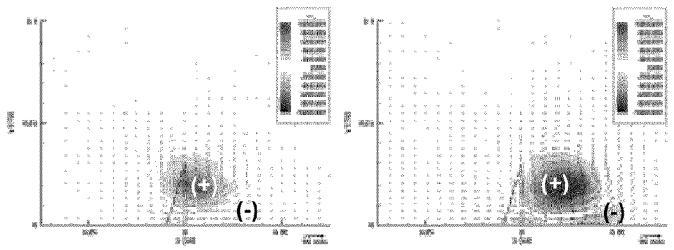

a) β_{VG}=10° b) β_{VG}=30°

Figure 8: Effect of skew angle for a solid vane VG at x= 10h. Longitudinal vorticity contours & secondary flow vectors.

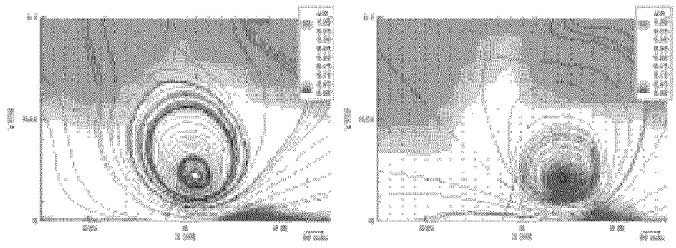

a) β_{VG}=10° b) β_{VG}=30°

Figure 9: Effect of skew angle for a solid vane VG at x= 10h. Longitudinal velocity contours & secondary streamlines.

As the vane VG is skewed to higher incidence angles, the primary vortex is strengthened, and is swept further in the lateral direction (*cf* Figure 8 & Figure 6c). We also see more of an effect on the boundary layer at higher incidences (*cf* Figure 9 & Figure 7c). However, the primary vortex is maintains about the same elevation ($0.7h$) for all cases. Only at the highest skew angle are any regions of significant negative vorticity observed, and only very near the wall (Figure 8b).

Integrating the vorticity over these planes to estimate total longitudinal circulation for VGs set at varying skew angles yields the expected results. The total circulation of a vane VG generally increases monotonically with increased skew angle to the freestream. (Figure 10). Note also that the total circulation dissipates in the downstream direction, and very rapidly in the region very near VGs when they are highly skewed.

Other procedures were also used to extract vorticity and circulation from the experimental data. The simplest of these methods was to use a line integral from the wall, through the vortex core, and out of the boundary layer. Providing that you know the lateral (z) location of the vortex, this estimate could be calculated using a single line of LDA data. For the vane VGs, this simple method produced roughly the same trends in circulation. Exceptions occurred very near the fin in the β_{VG}=20° case, where extrapolation of the unusually limited data set (for x<2cm) resulted in an exaggerated estimate of total circulation (see Figure 6a). Also, at high skew angles, it is typical for line integration to yield higher circulation estimates that whole-field integration, since this method neglects the region of negative fringe that appears on the up-flow side of the

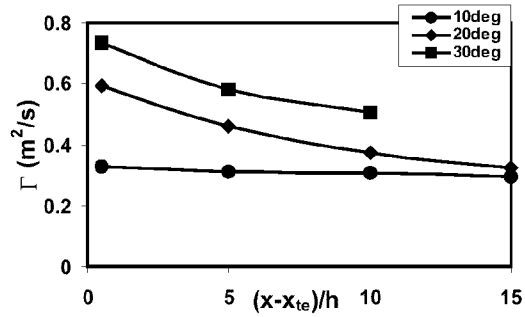

Figure 10: Trend in total longitudinal circulation for a 30mm×70mm delta-vane vortex generator.

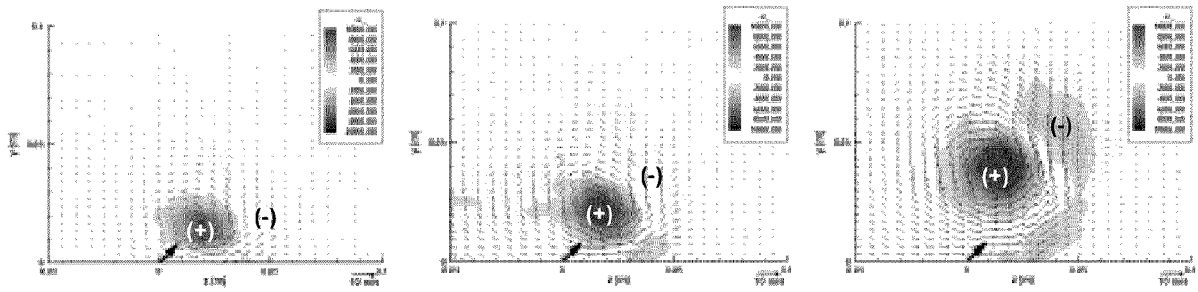

a) $VR = 1.38$ b) $VR = 1.84$ c) $VR = 2.70$

Figure 12: Effect of blowing rate for steady jet. Longitudinal vorticity contours & secondary flow vectors, $x = 20d$.

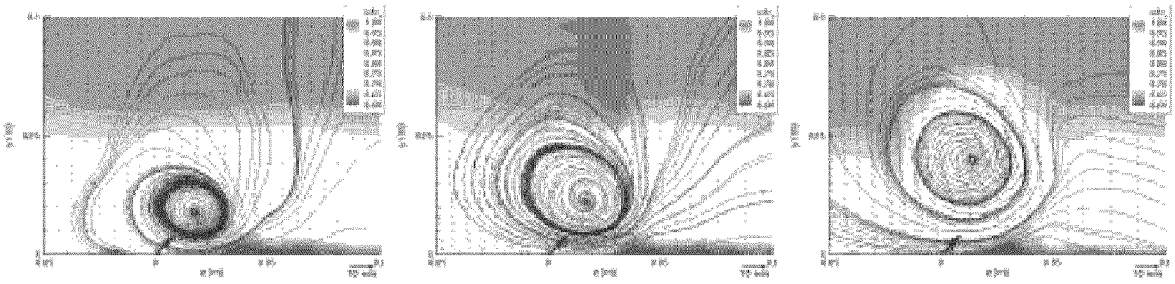

a) $VR = 1.38$ b) $VR = 1.84$ c) $VR = 2.70$

Figure 13: Effect of blowing rate for steady jet. Longitudinal velocity contours & secondary streamlines, $x = 20d$.

vortex. For the highest skew angle shown, the line integration method resulted in higher circulation than field integration on either the raw data (*CFD Analyzer*) or the interpolated data (Figure 11). As will be shown below, this "fringe vorticity" is often a major feature of the pulsed jet flowfield.

In summary, for solid vane vortex generators, the VG height determines the primary vortex elevation. The skew determines the vortex strength and lateral path. The strength of the vortex decreases monotonically in the downstream direction.

5.3 Steady Jet

A steady jet was first studied to provide a baseline for the pulsed jet results to be judged against, as well as to assess the influence of blowing magnitude independently. The blowing rate was varied from very low (VR–1.38) to the maximum that the air supply and flow meter could sustain.

The longitudinal vorticity and velocity fields are shown in Figure 12 and Figure 13, respectively, for a plane at x=20d for three different steady jet velocities. We can see that blowing rate has a direct impact on the location and initial strength of the primary vortex. This vortex, in turn, directly impacts the boundary layer by bringing high-energy fluid toward the wall. We can see qualitatively that the overall effect on the flowfield is somewhat proportional to the blowing magnitude.

Integrating the vorticity over the entire plane, indicates that the total circulation does not necessarily increase monotonically with increased blowing intensity (Figure 14a). If we simply judge effectiveness based on the total circulation produced by a vortex generator, we could overlook important attributes of the flowfield. If we limit the field of circulation integration to only regions of positive vorticity, we can isolate the influence of the primary vortex that is responsible for energizing the boundary layer, calculating its strength independently of secondary vortices. Doing so for the steady-jet measurements indicates that the primary vortex circulation does indeed increase monotonically with increased blowing intensity (Figure 14b). Identifying the proper 'measure of merit' to evaluate the *effectiveness* of varying types of vortex generators, without actually applying them to a separating flow, has not been as straight forward as one might hope.

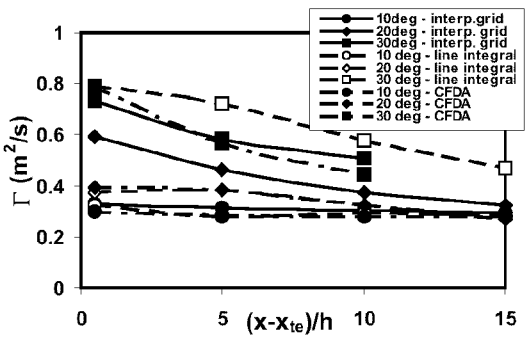

Figure 11: Effect of data reduction method on calculated circulation for 30×70mm vane vortex generator.

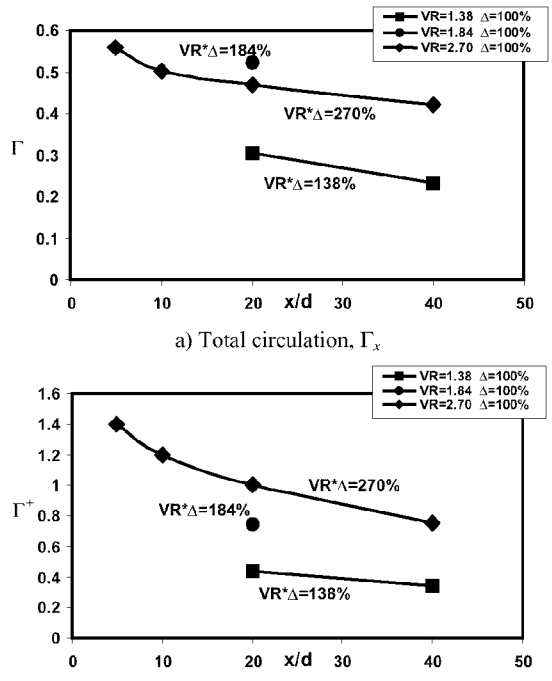

a) Total circulation, Γ_x

a) Positive part of circulation, Γ_x^+

Figure 14: Effect of blowing rate on longitudinal circulation.

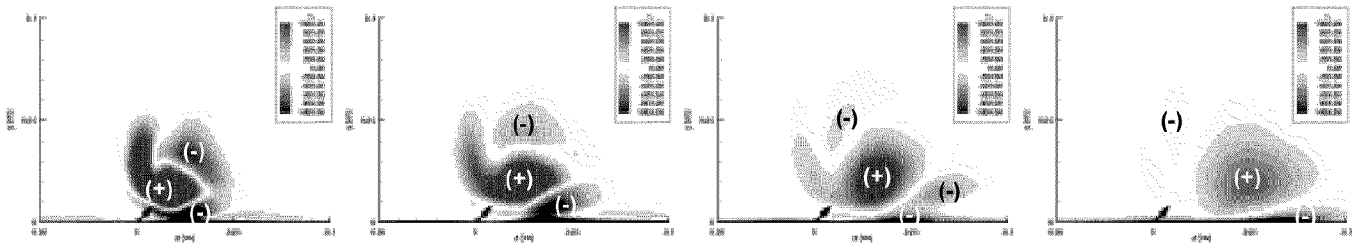

a) $x = 5d$ b) $x = 10d$ c) $x = 20d$ d) $x = 40d$

Figure 15: Computed Longitudinal vorticity contours for steady jet at VR=2.7.

The computational results are thus far limited to steady-state solutions of the RANS equations for steady-jet simulations. While the computational domain extends beyond the measurable region of the flowfield in the tunnel, only the measurable region is examined here. Note that in these simulations, the jet was directed at a 45° inclination from the *negative* z-axis. This is unfortunately in the opposite z direction than in the experiments.

The basic character of the predicted flowfield is much as reasoned by early research based on surface flow visualizations and intrusive experimental methods (Figure 16). Two vortices are initially created, as by a jet issuing normal to the surface. However, the vortex on the obtuse side of the jet is strengthened by the enhanced entrainment, and remains closer to the surface (Figure 15 & Figure 17). This vortex remains close to the surface, as the other moves away and dissipates. Ultimately only the stronger vortex remains, trailing close to the surface.

The simple algebraic turbulence model used does not account for the turbulent mixing of the jet itself, and is not capable of predicting the increased mixing caused by the jet. The turbulence of the jet flow itself is also overlooked. The net effects can be seen in the predicted vorticity field (Figure 15), which has many dissimilarities to vorticity field deduced from the experimental data. Most noticeable difference is that the predicted path of the primary vortex is too close to the wall. The predicted vortex trajectory is also too highly swept with respect to the freestream. The periodic boundary condition, which actually simulated an infinite lateral row of co-rotating jets spaced at $40d$, may be at least partially responsible for this.

Having said that, using this simple turbulence model did produce much more reasonable solutions than similar laminar predictions in which mixing was almost nonexistent. The primary expected features were predicted, and the overall effect on the boundary layer was rational.

The computed surface streamlines (Figure 18) are very similar to those computed by Zhang[7], who used a much more sophisticated turbulence model for the same jet geometry at a VR=2. They were calculated by seeding streamtrace particles in the first plane of data away from the wall, and constraining them to remain in that plane. It can be seen here that the primary vortex does not actually originate on the surface. The solutions reveal that most of the fluid in the primary vortex actually originates in the boundary layer ahead of the jet, passes very near the jet on the obtuse side, and is then entrained into the vortex.

Solutions have also been obtained at other jet velocities, and computations using two-equation turbulence models are underway. Based on the tentative success of these investigations, the next steps will include unsteady time-accurate simulations of the pulsed and steady jets. Since turbulence is a major contributor toward mixing, it is likely that successful time-accurate simulations of the PVGJ will require a better turbulence model. Two-equation (k-ε), algebraic Reynolds stress, and the Reynolds stress transport model have all been successfully used to simulate the steady jet flow field[7]. Of these, the latter was superior, provided that a good description of the upstream turbulent kinetic energy distribution was used.

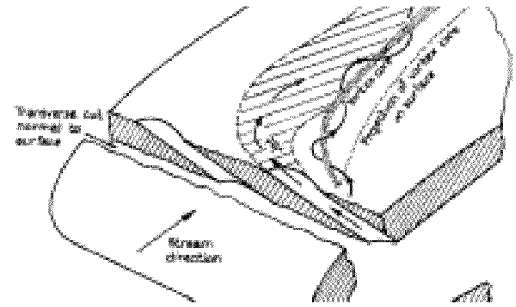

Figure 16: Sketch of steady VGJ flowfield (from reference 3).

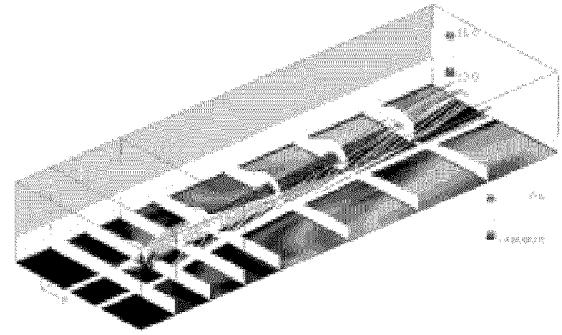

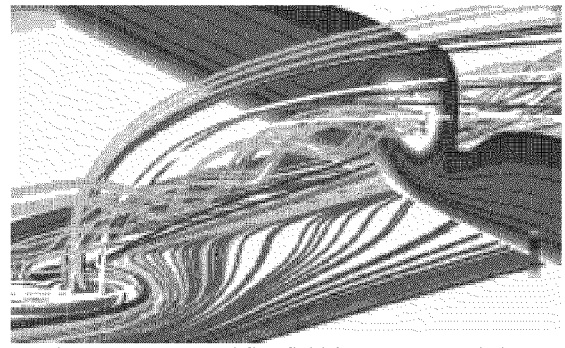

Figure 17: Computed flowfield for VR=2.7 steady jet.

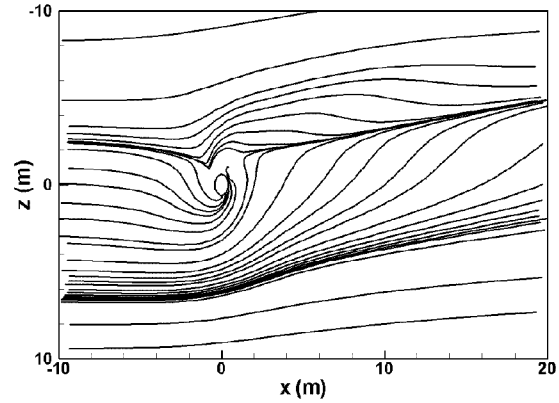

Figure 18: Computed surface limited streamlines (surface flow). VR=2.7 steady jet.

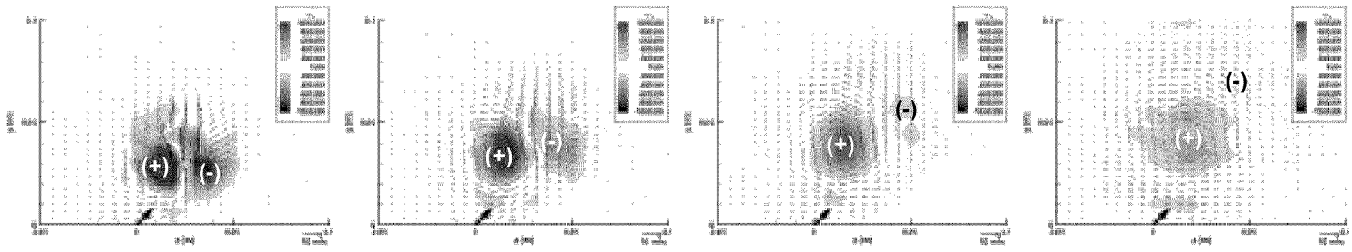

a) $x = 5d$ b) $x = 10d$ c) $x = 20d$ d) $x = 40d$

Figure 19: Longitudinal vorticity contours & secondary flow vectors. f=15Hz (F_x^+/ℓ = 0.5/m); VR=2.76; Δ=25%.

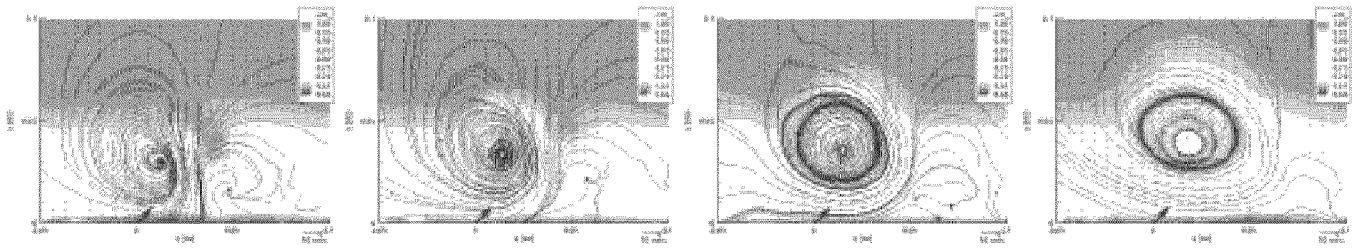

a) $x = 5d$ b) $x = 10d$ c) $x = 20d$ d) $x = 40d$

Figure 20: Longitudinal velocity contours, secondary streamlines. f–15Hz (F_x^+/ℓ – 0.5/m); VR–2.76; Δ–25%.

5.4 Pulsed Jet

If we want to increase the power of the steady jet, there are two obvious methods. We could simply blow harder (at higher velocity), or we could modulate (pulse) the flow. The latter alternative would enable a higher maximum jet velocity at the same average mass flow. Perhaps equivalent or superior performance could even be achieved at a reduced mass flow by pulsing at the same maximum velocity.

It is important to note that though this is a very dynamic time-varying flowfield, the results presented here are mean (time averaged) values. To extract unsteady phase-locked values or even dependable turbulence information at an equivalent number of locations would have required much more data to be taken. In the time since these experiments were conducted, the facility has been equipped with a much more powerful laser, putting turbulence quantities within reach in future experiments.

5.4.1 General Effects of Pulsed Blowing

We will first examine a typical case of an acceptably effective pulse velocity, at a moderate frequency and representative duty cycle (f–15Hz, VR–2.76, Δ–25%). In Figure 19, the mean longitudinal vorticity levels and secondary velocity vectors are shown at four measurement planes downstream of the jet. The longitudinal velocity contours are shown with secondary streamlines in Figure 20. It is observed that very near the jet, there are large positive and negative vorticity levels, very similar to those observed near the solid VG shown above. However, in this case, the primary vortex is established slightly higher in the boundary layer, and it moves slowly away from the wall as it proceeds downstream. It is also seen that the peak vorticity level in the growing primary vortex (marked with (+)) is decreasing as it the observation plane is moved downstream. However, the negative vorticity "fringe" appears to vanish almost completely by the last measurement station. The sum effect is that the total longitudinal circulation is actually *increasing* at the end of the measurement region (Figure 21a). This phenomenon is not at all typical of steady vortex generation devices, including steady blowing. However, if we limit the field of integration to the region of positive vorticity, we observe the dissipative behavior similar to solid vanes (Figure 21b).

Examining the velocity contours at these planes (Figure 20) indicates that it is affecting the outer boundary layer in a similar manner as solid VGs, but seems to be affecting the inner boundary layer less. It is difficult to make definitive conclusions regarding inner boundary layer behavior and stability based solely on these data.

Comparing to steady blowing at twice the mean flow rate (VR=1.38), we have decreased the total longitudinal circulation proportionally to the reduction in mean mass flow rate (Figure 21a). However, we have actually *increased* the circulation in the primary vortex significantly (Figure 21b). This apparent contradiction is due to the negative vorticity in the pulsed jet case that is not significant under the influence of the steady jet at this velocity ratio (*cf* Figure 19c & Figure 12a). Also, the pulsing has moved the vortex core significantly farther away from the wall. It has been observed in these experiments that the primary influence on the position of this vortex is the maximum jet velocity, whether the jet is pulsed or not.

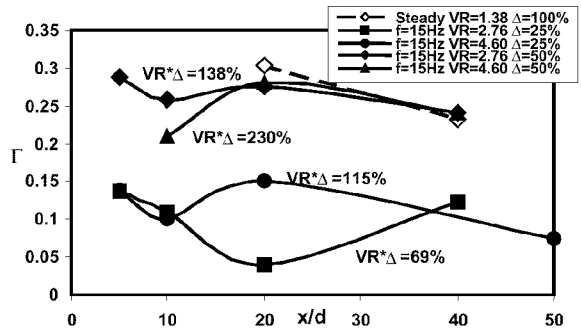

a) Total circulation, Γ

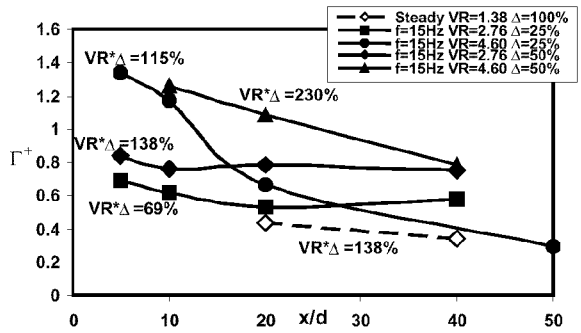

b) Positive part of circulation, Γ^+

Figure 21: Longitudinal trend in total longitudinal circulation. f=15Hz (F_x^+/ℓ = 0.5/m)

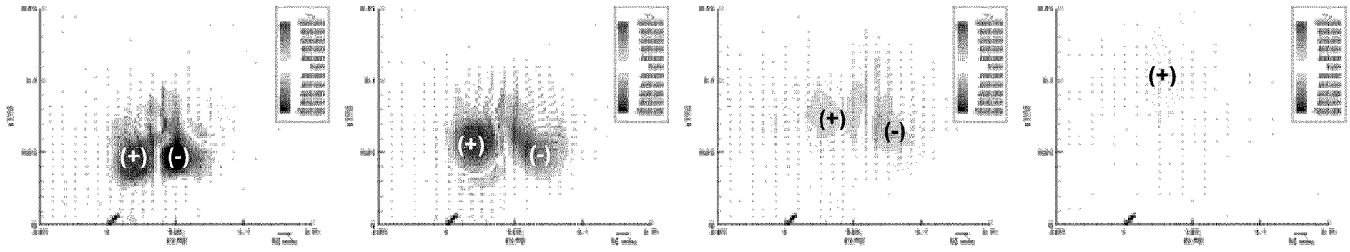

a) $x = 5d$ b) $x = 10d$ c) $x = 20d$ d) $x = 50d$

Figure 22: Longitudinal vorticity contours & secondary flow vectors. f=15Hz (F_x^+/ℓ = 0.5/m); VR=4.60; Δ=25%.

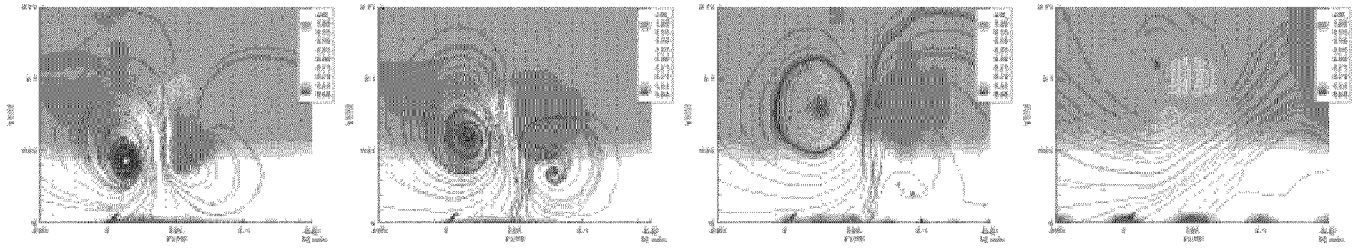

a) $x = 5d$ b) $x = 10d$ c) $x = 20d$ d) $x = 50d$

Figure 23: Longitudinal velocity contours & secondary streamlines. f=15Hz (F_x^+/ℓ = 0.5/m); VR=4.60; Δ=25%.

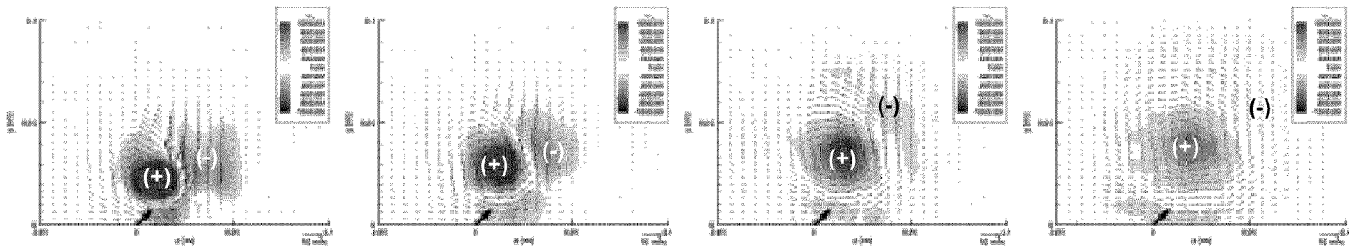

a) $x = 5d$ b) $x = 10d$ c) $x = 20d$ d) $x = 40d$

Figure 24: Longitudinal vorticity contours & secondary flow vectors. f–15Hz (F_x^+/ℓ – 0.5/m); VR–2.76; Δ–50%.

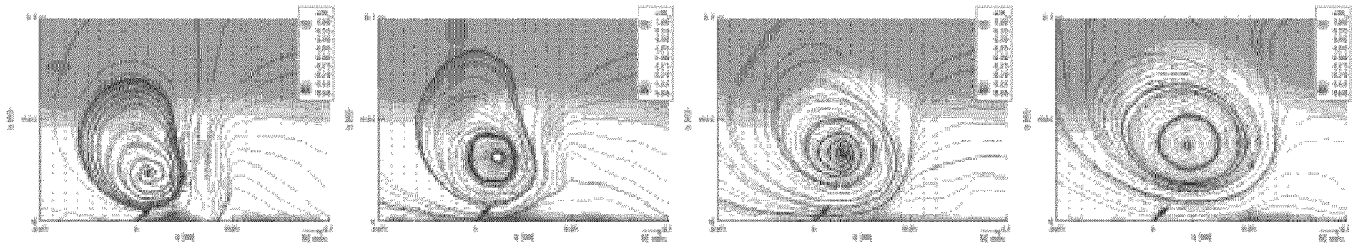

a) $x = 5d$ b) $x = 10d$ c) $x = 20d$ d) $x = 40d$

Figure 25: Longitudinal velocity contours & secondary streamlines. f=15Hz (F_x^+/ℓ = 0.5/m); VR=2.76; Δ=50%.

5.4.2 Stronger Pulses

Using the unsteady case described above as a point of reference; there are a limited number of ways that we can attempt to increase the effectiveness of the PVGJ. Perhaps one's first thought is to simply blow harder. The destructive effects of increasing the blowing magnitude too much (VR=4.60) are apparent in Figure 22 & Figure 23. The calculated total circulation values (Figure 21a), imply that the vortex starts out about the same strength but quickly grows stronger than the VR=2.76 case. However, as seen in Figure 23, the vortex's trajectory soon takes it completely out of the boundary layer where it is overcome by the freestream momentum, then quickly dissipates (Figure 21).

5.4.3 Longer Pulses

We could instead attempt to increase effectiveness by increasing the duty cycle. Doubling the duty cycle (to Δ=50%) effectively doubles the total mass-flow rate from the jet. In doing so, we observe that the vortex is no longer ejected from the boundary layer, even though the overall mass flow rate is a bit higher than the previous case. (Figure 25). The vortex maintains essentially the same trajectory as it did at half the duty cycle (Δ=25%), though the overall circulation has approximately doubled (Figure 21). Note however, that the circulation is again *decreasing* by the time it gets 40d downstream of the jet. Also, there is only a 35-45% increase in primary vortex circulation at a cost of 100% more mass flow rate (Figure 21b)

5.4.4 Stronger and Longer Pulses

The effects of increasing both the jet velocity and the duty cycle simultaneously were also examined at the same frequency (VR=4.6, Δ=50%). This produced nearly the same total circulation as only 60% the velocity (Section 5.4.1) and mass flow, at the same duty cycle (Figure 21a). The primary vortex circulation starts at about the same level as it did for the same velocity ratio at half the duty cycle (Figure 21b). This high circulation level was sustained for a slightly longer distance, but ultimately was dissipated at a similar rate. By the x=40d location, the primary vortex was no stronger than it was for the same duty cycle at 60% the jet velocity (Section 5.4.3), and dissipating much more rapidly.

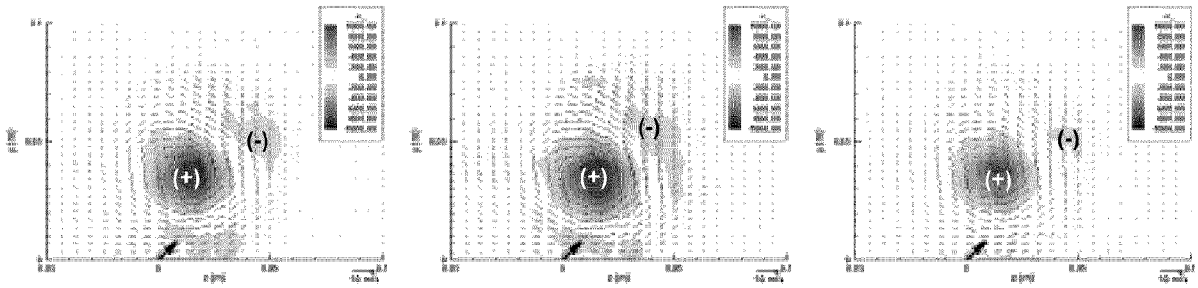

a) f=7Hz (F_x^-/ℓ = 0.25/m) b) f=15Hz (F_x^+/ℓ = 0.5/m) c) f=30Hz (F_x^+/ℓ = 1.0/m)

Figure 26: Longitudinal vorticity contours & secondary flow vectors. x=20d; VR=2.76; Δ=50%.

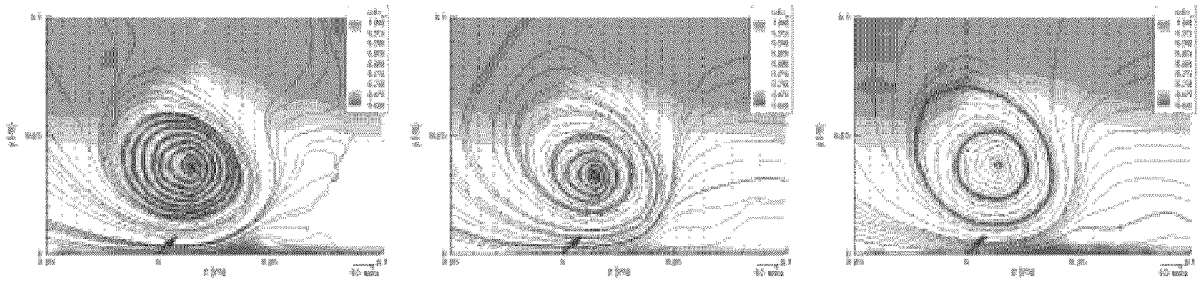

a) f=7Hz (F_x^-/ℓ = 0.25/m) b) f=15Hz (F_x^+/ℓ = 0.5/m) c) f=30Hz (F_x^+/ℓ = 1.0/m)

Figure 27: Longitudinal velocity contours, secondary streamlines. x=20d; VR=2.76; Δ=50%.

5.4.5 Effects of Frequency

It is understood from past experience that frequency is a major factor when controlling separation in flows having dominant length scales. For example, in the case of trailing edge separation on an airfoil, the distance from the actuator to the trailing edge is the critical length scale that the frequency must be 'tuned' to. In this experiment there is no length scale, or even separation, to control. However, there did appear to be optimum frequencies for both generating circulation in the primary vortices, and maintaining it.

Using only the cases where VR*Δ=138% (constant mass flow rate) for comparison, the time-averaged primary vortex position and boundary layer edge profile remain relatively unchanged over the range of frequency tested (Figure 27). The pulsed vortex does have a substantially different path than for the steady jet though (*cf* Figure 12a). The total circulation is also relatively unaffected, and at no frequency was the total circulation greater that for the steady case (Figure 28a). However, pulsing always generated a stronger primary vortex than the steady jet (Figure 28b). There is significant variation due to frequency in the primary vortex circulation, with 15Hz clearly superior to the other frequencies investigated.

6 CONCLUDING REMARKS

Based on these experiments, we can make a few general observations about the effects of various jet parameters on the PVGJ flowfield, and its effect on an attached boundary layer.

The path of the primary vortices appears to be primarily a function of the maximum pulse velocity, or the velocity ratio. On can certainly blow too little to have an appreciable effect. Conversely, to high of jet velocity can be applied, forcing the resultant vortices out of the boundary layer, resulting in great losses in effectiveness. Persistence of the circulation requires the vortex to remain in the boundary layer. If the vortex pulses leave the confines of the boundary layer, they are quickly overcome by the freestream momentum and dissipated.

The analysis has raised questions as to what might be the best 'measure-of-merit' for PVGJs in an un-separated flow. Basing judgments of effectiveness on the total circulation produced by a vortex generator can lead to different conclusions that looking at only the strength of the primary vortex, which is responsible for energizing the boundary layer.

Strength of the primary vortex is essentially a function of the time-average mass flow rate (i.e. the time-averaged energy that is being added to the flow). Pulsing is effective way to produce persistent vortices while greatly reducing mass flow. Pulsing significantly increases the strength of the primary vortex. For example, pulsing the jet at 50% duty resulted as much as twice the mean circulation in the primary vortex as steady blowing at the same average mass flow rate. When the duty cycle was reduced to 25% at the same pulse velocity, the primary vortex was still stronger that the steady jet, was more persistent, and required half the mass flow rate.

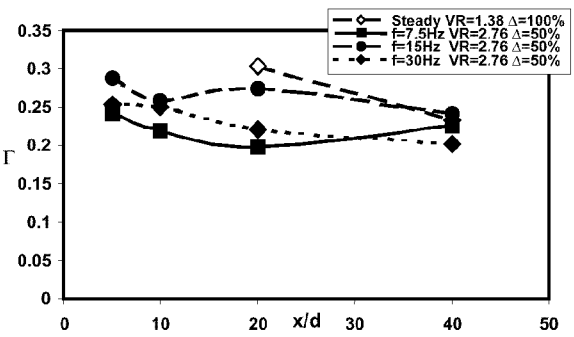

a) Total circulation, Γ

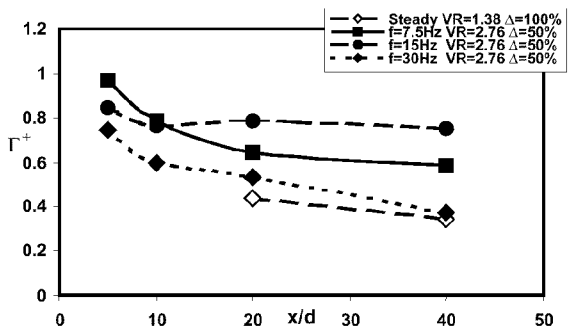

a) Positive part of circulation, Γ^+

Figure 28: Effect of frequency on longitudinal circulation.

7 FUTURE DIRECTION

The results from this boundary layer investigation have already been used to guide further validation work in a large-scale high-speed demonstration of separation control. Here, the PVGJ concept was integrated into an existing airfoil model (the DERA M2303) for a slightly different application for separation control. The primary emphasis was on reducing the loss of lift and drag rise due to shock-induced separation on transonic airfoils. These high Reynolds number transonic (M≈0.7) tests were conducted in the DERA Bedford 8ft×8ft High Speed Tunnel. Passive sub-boundary layer control devices developed at DERA were also investigated. These techniques offer a large potential for reducing boundary layer flow separation (and thus drag) behind the upper surface shock wave.

Future goals of the PVGJ analysis discussed in this paper include continuing the CFD effort to include unsteady time-accurate simulations of the pulsed and steady jets. Since turbulence is a major contributor toward mixing, it is likely that successful time-accurate simulations of the PVGJ will require a better turbulence model. Two-equation (k-ε), algebraic Reynolds stress, and the Reynolds stress transport model have all been successfully used to simulate the mean flow field[7]. Of these the latter was superior provided that a good description of the upstream turbulent kinetic energy distribution was used. A reduced order modeling effort is also being initiated, which will use the experimental and computational results to develop analytical models for PVGJs to be used in design studies.

REFERENCES

[1]Wallis. R.A., "The Use of Air Jets for Boundary Layer Control," Aero. Note 110, Aerodynamics Research Laboratories, Melbourne, Australia, Jan 1952.

[2]Wallis. R.A., "A Preliminary Note on a Modified Type of Air-Jet for Boundary Layer Control," Current Paper No. 513, Aeronautical Research Council, Australia, 1960.

[3]Pearcey, H.H., "Shock Induced Separation and its Prevention," in *Boundary Layer & Flow Control, Vol. 2*, Ed. G.V Lachmann, Pergamon Press, New York, pp. 1170-1344, 1961.

[4]Johnston, J.P., & Nishi, M., "Vortex Generator Jets – A Means for Flow Separation Control," *AIAA Journal*, 28:989, 1990.

[5]Compton, D.A., & Johnston, J.P., "Streamwise Vortex Production by Pitched and Skewed Jets in a Turbulent Boundary Layer," *AIAA Journal*, 30:640, 1992.

[6]Selby, G.V., Lin, J.C., & Howard, F.G., "Control of Low-Speed Turbulent Separated Flow Using Jet Vortex Generators," *Experiments in Fluids*, 12:394, 1992.

[7]Zhang, X., Zhang, H-L, & Collins, M.W., "Some Aspects of Streamwise Vortex Production Using Air Jets," *AIAA-96-0209*, January 1996.

[8]Peake, D.J., Henry, F.S., & Pearcey, H.H., "Viscous Flow Control with Air-Jet Vortex Generators," *AIAA-99-3175*, June 1999.

[9]Hasegawa, H., Matsuuchi, K., & Tanaka, J., "Development of an Active Separation Control System Using Vortex Generator Jets," 3rd ASME/JSME Joint Fluid Engineering Conference, *FEDSM99-6944*, San Francisco, California, July 18-23 1999.

[10]Khan, Z.U. & Johnston, J.P., "On Vortex Generating Jets," *1st International Symposium on Turbulence and Shear Flow Phenomena*, Santa Barbara, Sept. 12-15 1999.

[11]Johnston, J.P., "Pitched and Skewed Vortex Generator Jets for Control of Turbulent Boundary Layer Separation: a Review," 3rd ASME/JSME Joint Fluids Engineering Conference, *FEDSM99-6917*, San Francisco, CA, July 18-22 1999.

[12]McManus, K., et al., "Pulsed Vortex Generator Jets for Active Control of Flow Separation," AFRL Technical Report *AFRL-VA-WP-TR-1998-3082*, November 1997.

[13]McManus, K., Joshi, P.B., Legner, H.H., & Davis, S.J., "Active Control of Aerodynamic Stall Using Pulsed Jet Actuators," *AIAA-95-2187*, June 1995.

[14]McManus, K., Ducharme, A., Goldley, C., & Magill, J., "Pulsed Jet Actuators for Suppressing Flow Separation," *AIAA-96-0422*, January 1996.

[15]McManus, K. & Magill, J., "Separation Control in Incompressible and Compressible Flows using Pulsed Jets," *AIAA-96-1948*, June 1996.

[16]McManus, K. & Magill, J., "Airfoil Performance Enhancement Using Pulsed Jet Separation Control," *AIAA 97-1971*, June 1997.

[17]Magill, J. & McManus, K., "Control of Dynamic Stall using Pulsed Vortex Generator Jets," *AIAA 98-0675*, January 1998.

[18]Seifert, A., Bachar, T., Koss, D., Shepshelovich, M., & Wygnanski, I., "Oscillatory Blowing, a Tool to Delay Boundary Layer Separation," *AIAA Journal*, 31:11, pp.2052-2060, 1993.

[19]Seifert, A., Darabi, A., & Wygnanski, I., "On the Delay of Airfoil Stall by Periodic Excitation," *Journal of Aircraft*, 33:4, pp. 691-699, 1996.

[20]Seifert, A. & Pack, L.G., "Oscillatory Control of Separation at High Reynolds Numbers," AIAA Journal, 37:9, pp. 1062, Sep 1999.

[21]Seifert, A. & Pack, L.G., "Active Control of Separated Flows on Generic Configurations at High Reynolds Numbers," *AIAA 99-3403*, June 1999.

[22]Johari, H. & McManus, K., "Visualization of Pulsed Vortex Generator Jets for Active Control of Boundary Layer Separation," *AIAA 97-2021*, June 1997.

[23]Tilmann, C.P. & Osborn, R.F., "Active Flow Control for Drag Reduction at AFRL's Aerodynamic Configuration Branch," *Proceedings of the 17th Canadian Congress of Applied Mechanics*, Hamilton, Ontario, June 1999.

[24]Tilmann, C.P. & Osborn, R.F., "Active Control of Separation at AFRL's Aerodynamic Configuration Branch," *Proceedings of the 17th Canadian Congress of Applied Mechanics*, Hamilton, Ontario, June 1999.

[25]"*New World Vistas — Air and Space Power for the 21st Century*," USAF Scientific Advisory Board, 1995.

[26]Wheeler, G.O., "Means of maintaining attached flow of a flow medium," US patent No 4455045, 1984.

[27]Wheeler, G.O., "Low drag vortex generators," US Patent No 5058837, 1991.

[28]Lin J.C., "Control of turbulent boundary-layer separation using micro-generators," *AIAA-99-3404*, 30th AIAA Fluid dynamics conference. June 1999.

[29]Yanta, W.J., "A Three-Dimensional Laser Doppler Velocimeter (LDV) for Use in Wind Tunnels," *Proceedings of 8th International Congress of Instrumentation in Aerospace Simulation Facilities*, Monterey, California, pp. 294-301, 1979.

[30]Dantec Measurement Technology A/S, "Principles of LDA," [*http://www.dantecmt.dk*]

[31]Amtec Engineering Inc., ©1988-2000 [*http://www.amtec.com*]

[32]Baldwin, B.S. and Lomax, H., "Thin Layer Approximation and Algebraic Model for Separated Turbulent Flow," *AIAA-78-0257*, January 1978.

[33]"*The General Aerodynamic Simulation Program, Version 3 Users Manual*," Aerosoft Inc., Blacksburg, Virginia. 1996.

[34]van Leer, B., "Flux-Vector Splitting for the Euler Equations," *Lecture Notes In Physics*, Vol. 170, 1980.

[35]Hirsch, C., "*Numerical Computation of Internal and External Flows, Volumes 1 and 2*," John Wiley and Sons, 1992.

Paper #5
Q by N. Malmuth: Is DNS contemplated for this problem? Will laminar jets be considered?

A. (Tilmann) LES and DNS are contemplated for this problem, but significant computational resources will be required. Even when considering steady jets, it has been shown that using correct turbulence models accounting for Reynolds stress transport and including good turbulence profiles at the boundaries (at the jet and in the boundary layer) are crucial.
Laminar jets are not being considered at this time. The pulsed nature of the jet would also introduce many uncertainties for a laminar jet laboratory experiment.

Q (Mr. E. Collin): What about the reliability of the LDA mean flow results, since the seeding is done upstream of the pulsed VGJ's valve [in the freestream]?

A (Tilmann): In fact, we seeded the PVGJs themselves. The freestream was also eventually seeded due to the return design of the wind tunnel.

This page has been deliberately left blank

Page intentionnellement blanche